18TH WORLD CONFERENCE ON EARTHQUAKE ENGINEERING
WCEE2024
MILAN

MILAN, ITALY
30TH JUNE - 5TH JULY 2024

www.wcee2024.it

SEISMIC LOSS ASSESSMENT OF EXISTING HOTEL BUILDING IN ECUADOR

J. Poveda[1], G.J. O'Reilly[2]

[1] Centre for Training and Research on Reduction of Seismic Risk (ROSE Centre), Scuola Universitaria Superiore IUSS di Pavia, Italy, jose.poveda@iusspavia.it

[2] Centre for Training and Research on Reduction of Seismic Risk (ROSE Centre), Scuola Universitaria Superiore IUSS di Pavia, Italy

Abstract: *This paper presents results from a seismic loss assessment of an existing hotel structure located in Quito, Ecuador using a storey-loss-based assessment methodology. The building, constructed in the late 1950s and considered a city landmark, has undergone several renovations and repairs, but not yet a seismic retrofit. A detailed building investigation was conducted, and extensive data on structural layout, dynamic characteristics, and damageable inventory were collected and utilised. The building models were validated against ambient noise vibrations, and fragility functions and vulnerability curves were derived from non-linear analyses and the collected loss data. The results showed that the building has a notable level of expected annual losses, primarily due to non-structural loss. Overall, the study results provide a benchmark example for conducting seismic loss assessment of non-code-compliant and other vulnerable structures in Ecuador, and the South American context in general.*

1 Introduction

Performance-based seismic assessment of existing buildings is inherently complex due to the diverse structural typologies, construction materials, and historical building practices worldwide. These structures often lack original design documents and are seismically vulnerable since they predate modern seismic design standards. Consequently, assessments must rely on site-specific data, field surveys, and advanced analysis techniques to reduce the uncertainties associated with these historical constructions. Performance-based methodologies provide a means to assess any typology by explicitly considering its inherent uncertainties, as described in FEMA P-58 (2018), for example, or in an implicit manner, such as ASCE 41 (2017). Still, technical difficulties related to the specifics of the existing building may always need to be addressed by local experts.

The seismic vulnerability of existing buildings is a critical concern in regions with a history of high seismic activity, such as Ecuador. In this paper, we focus on a cultural heritage building, which is a hotel with local historical and architectural significance. Assessing its seismic vulnerability and developing mitigation strategies are not only a matter of safeguarding public safety but also preserving valuable cultural heritage. While they may be considered as low-risk or normal occupancy building, as per ASCE 7 (2017) and NEC-15 (2014), respectively, their collapse or demolition may have a tremendous impact on cultural identity. Depending on local legislation, the decision to retrofit usually rests the building owner.

This paper presents a case study of an iconic hotel situated in Quito, Ecuador. The building was erected during the late 1950s and has undergone various modifications and reparations over the years, yet seismic retrofitting remains an unaddressed concern. The assessment encompasses a detailed seismic hazard analysis with hazard-consistent ground motion selection following state-of-the-art approaches. Field surveys, material tests and ambient noise vibrations are used to develop a non-linear numerical model to perform multiple stripe analysis (MSA) to characterise Engineering Demand Parameters (EDP) needed to estimate losses due to required repair costs. Moreover, a damageable inventory is compiled based on detailed knowledge available

from the building owners and collaboration with local experts with corresponding fragilities and repair costs to construct storey loss functions (SLFs). Furthermore, structural fragilities following ASCE 41 (2017) damages state and collapse criteria are constructed, as local legislation refers primarily to this document. Finally, vulnerability, together with Expected Annual Losses (EAL) as Decision Variables (DVs), are estimated, which represent a key tool for decision-makers. Discussion of the results delves into the need for further research on the structural typology and the need to develop proper strategies to reduce collapse and losses in this region.

2 Case study

2.1 Description of building

The building is part of a more extensive complex of structures of an elongated hotel located in Quito, Ecuador (Figure 1). The main hotel building was constructed in the late 1950s, and later expansions were mainly attached in the northern side, with each block possessing a structural joint on the superstructure level. It initially comprised five architectural blocks, with a constructed area of approximately 15,400 m². Visual inspections revealed several key structural characteristics for each block. In particular:

- North Block: This comprises a two-storey mixed-use structure with reinforced concrete (RC) walls and steel beams at the ground floor level, steel trusses for roof, and solid concrete slabs for both levels. It mainly comprises rental event halls, lobbies, bathrooms, service corridors, storage rooms and offices.
- Central Block: The central block, with two underground floors, seven storeys and accessible terrace, is primarily constructed using RC. It features perimeter columns, concrete core walls for staircases and elevators, and unidirectional slabs supported by embedded beams. Underground floors are used for hotel infrastructure as equipment, services, storage rooms, employee canteen and more rental event halls. The ground floor encompasses the reception, offices, and retail stores. Middle storeys are used for hotel rooms, the top storey is a restaurant, and the roof is for elevator equipment.
- South and South-South Blocks: Each block has an additional structural joint in the middle, resulting in a total of four structural blocks. These structures, each three storeys high with one half confined underground floor, are constructed using RC with either unidirectional or solid slabs. Additionally, no shear walls were identified but stiff infills framed by non-conforming code columns. These blocks are used mainly as hotel rooms, corridors, offices, or storage.
- Bungalow Blocks: Three independent one-storey structures made of RC with unidirectional slabs with stiff infills framed by non-conforming code columns. These blocks serve as small departments for rental. It is important to mention that amenities such as gardens, pools, saunas, and parking lots are on the building exteriors; hence, they are not described.

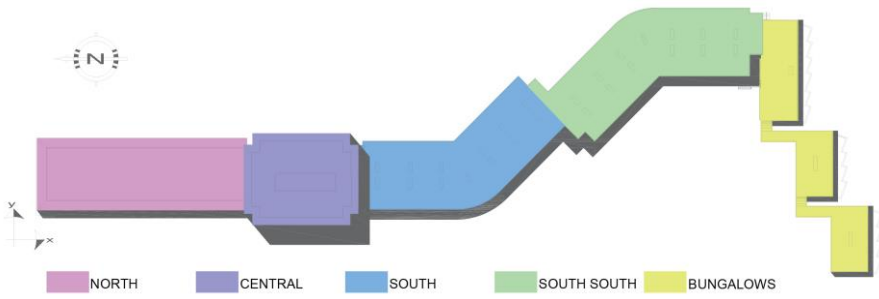

Figure 1. Plan distribution scheme of the various hotel blocks

Soil properties, material strength, typical reinforcement details and ambient noise vibrations were executed by local experts. It is essential to emphasise that the hotel is an existing structure constructed over 60 years ago and was not seismically designed. At the date of construction, there was no building code in place and common practice was to design for gravity loads similar to other parts of the world. Notable differences compared to modern structures were found, including the use of smooth reinforcement bars, wider spacing of stirrups (>20 cm), bar overlaps in areas near joints, and a lack of specific considerations for joint connections. Such structures are categorised as highly vulnerable by simpler assessments such as Tier 1 and Tier 2 on ASCE 41 (2017), and non-ductile behaviour is expected during seismic loading.

The present study was limited to the central block shown in Figure 2a primarily due to computational constraints; however, the study's relevance remains valid because the building concentrates on the essential

functions and infrastructure of a hotel. Moreover, structural joints between structural blocks permit the decoupled analysis. Furthermore, fixed-based behaviour at ground level was assumed due to the relatively high stiffness of the underground floors provided by the basement walls, so only above-ground levels were considered for the analysis, as shown in the structural analysis model in Figure 2b.

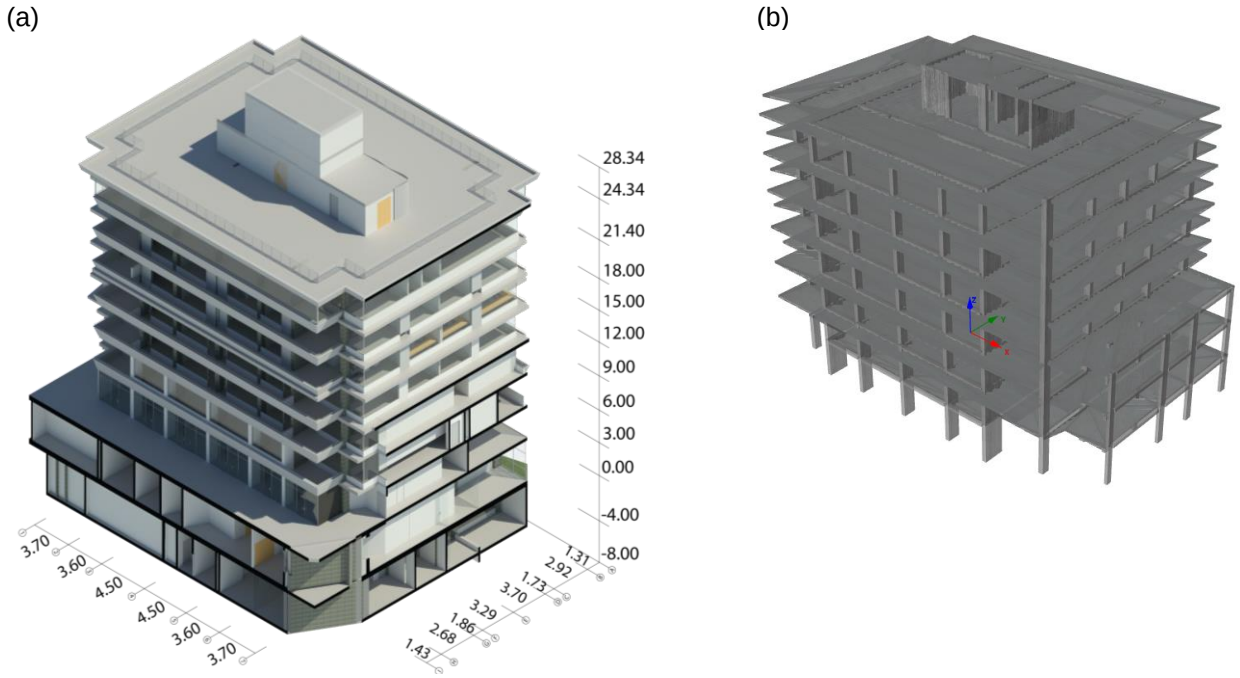

Figure 2. Illustration of the (a) architectural layout in meters and (b) structural modelling of the case study block

2.2 Damageable inventory and repair costs

To illustrate how a more refined but expedited loss assessment could be implemented within this context, a damageable inventory was extracted from the available documents and field surveys, similar to other studies, such as Nafeh and O'Reilly (2023). In parallel, a detailed 3D model was generated to facilitate Building Information Modelling (BIM) integration to visualise and group components and estimate quantities. This inventory comprised data related to the non-structural elements like mechanical and electrical equipment, piping, partition walls, contents, sanitary units and façade elements. The BIM integration proved very effective in grouping and identifying component groups and quantities, facilitating the interaction with the local experts to identify refined estimates of repair costs. To effectively manage this extensive catalogue of elements, a systematic categorisation approach was employed. Initially, the inventory was organised into two main categories: structural and non-structural elements.

Due to the non-structural elements (NSE) inventory's complexity and size, a further sub-grouping of NSEs was developed, recognising similarity between NSEs. For instance, instead of categorising door elements based on dimensions, of which there are many in the hotel building, a practical grouping approach was adopted. Doors were classified into exterior, interior, or emergency types, reflecting their distinct functions and similarity in repair or replacement cost. This grouping strategy enhanced the usability and clarity of the inventory, ignoring small variability that would make the exercise more cumbersome.

Fragility functions characterising each elements seismic vulnerability were defined using several sources, including FEMA P-58 (2018) and expert opinion from local practitioners. Damage correlation between elements was considered in the analysis. For instance, room contents expected to be damaged by flooding were assumed to be impacted by the fragility of piping distribution systems located nearby. Finally, repair and replacement costs were compiled by a local expert, who conducted a detailed pricing analysis for the specific units and country contexts of the project, which fits better than consequences database from other regions when local data is not available or collected. This inventory provides actual data, which is enriched by understanding the as-built conditions of the structure under investigation. Table 1 gives a macro-summary of

the categories, but more detailed information can be found via an electronic supplement available at: https://gerardjoreilly.github.io/publications/.

2.3 Numerical modelling

The numerical modelling used the commercially available software (SeismoSoft, 2023) to assess structures with fibre-section and force-based elements. For the steel reinforcement hysteretic model, the Menegotto-Pinto material model was selected, characterised by a degraded strength $f_{s-deg} = 210\ MPa$ derived from the expected yielding stress $f_{y,e} = 318\ MPa$ as recommend by ASCE 41 (2017) was adopted. This reduction represents the stress at slippage of smooth bars with shorter development length l_d. The elastic modulus was assumed $E_s = 200GPa$ and a 0.5% post-yielding stiffness was used. It is noted that limited information was available for the rebar since no destructive tests were performed; lap splice length and location are assumed as the worst case but were not systematically verified in-situ. For the concrete hysteretic model, the Mander et al., (1988) material model was used, considering concrete elastic modulus $E_c = 25GPa$ and an expected compressive strength of $f_{c,e} = 30\ MPa$, verified with destructive and non-destructive tests performed in-situ. For the confinement of the core and cover concrete materials, a factor of $k = 1$ was defined since no seismic details and widely spaced hoops were observed in-situ.

Table 1. General information on the damageable inventory catalogue

Description	Source	Cod.	EDP	Repair Cost Unit
Non-conforming moment frame with inadequate development of reinforcing	FEMA P-58	B1041.132b	PSD[1]	unit (per node)
Low-rise RC walls with return flanges	FEMA P-58	B1044.043	PSD[1]	m^2
Monolithic cast-in-place stairs with no seismic joints	FEMA P-58	C2011.021b	PSD[1]	unit
Gypsum infill wall	FEMA P-58	C3011.001a	PSD[1]	m^2
Brick Infill wall	Cardone & Perrone (2015)		PSD[1]	m^2
Glazing	User		PSD[1]	m^2
Doors (Interior, exterior, emergency)	User		PSD[1]	m^2
Bathroom contents and electric connections	User		PSD[1]	m^2
RC parapet	User		PFA[2]	m^2
Piping systems – water distribution	FEMA P-58	D2021.011a	PFA[2]	m
Sanitary waste piping	FEMA P-58	D2031.011b	PFA[2]	m
Vapor piping distribution	User	D2061.011a	PFA[2]	m
Piping systems – gas distribution	User		PFA[2]	m
Elevator	FEMA P-58	D1014.012	PFA[2]	unit
Transformation chamber	FEMA P-58	D5011.011a	PFA[2]	unit
Distribution panel	FEMA P-58	D5012.031a	PFA[2]	unit
HVAC galvanized sheet metal ducting	FEMA P-58	D3041.011a	PFA[2]	kg
HVAC fan independently supported but not on vibration isolators	FEMA P-58	D3041.002a	PFA[2]	unit
Equipment	User		PFA[2]	unit
Contents	User		PFA[2]	m^2

[1] *Peak Storey Drift*

[2] *Peak Floor Acceleration*

To model the structural members, the numerical model utilised force-based elements with more than 150 fibres for the beam and column, and more than 300 fibres for wall elements. For columns and beams, a plastic hinge length of 16% of the element length was defined (Scott and Fenves, 2006). This choice is common practice and represents the observed plastic hinge lengths in laboratory tests and post-earthquake field inspections (Calabrese et al., 2010). For walls, a full-length distributed plasticity for the elements to ensure a general representation of their response (Odabaşı, 2020) was employed where flexural yielding is expected since $h_w/l_w > 2.0$. Shear-flexure interaction and shear failure modes were not accounted for directly since it was deemed beyond the scope of this work to precisely model the walls shear degradation. Instead, the shear

response was modelled elastically and the shear capacity of the elements was estimated according to ACI 318 (2019). Shear failures are not registered until medium or high ductility demands which is assumed to have small incidence in the demand parameters of interest. The floor slab was defined as a rigid diaphragm. The embedded one-way beams were modelled as identified in the field for the rotational stiffness contribution to the joint and vertical load distribution. Rigid ends in the columns were assigned to account for the joint stiffness contribution. Additionally, rigid links between linear segments of the core walls, such as those found in stairwells and elevators, were assigned to realistically capture their interaction since they were monolithically built.

A modal analysis was performed and the results are listed in Table 2, showing good agreement with the dynamic properties measured via sensors installed on the actual building. Furthermore, the deformed shape for the first controlling modes was also verified with additional ambient noise vibrations measurement. Interesting to note is that Mode 1 has a 46.31% effective modal mass in the X-direction and 11.88% in the Y-direction and Mode 2 has a 5.99% effective modal mass in the X-direction and 48.7% in the Y-direction, and both are not widely spaced. This information helped to clarify the ambient noise vibration measurements, which showed that two vibration periods were closely recorded, and a torsional deformation mode was identified via extra sensors placed in the corners and not solely close to the centre of mass of each storey. Regarding the damping values measured from the in-situ measurement, these are also reported in Table 2. The damping ratio estimated using the half bandwidth approach showed damping values in the 1.6 to 3.5% range, which is slightly lower than the typically assumed value of 5%. For the numerical analysis, a Rayleigh damping model was thus defined with a 4% damping ratio for the first mode and a 6% damping ratio for the third mode.

Table 2. Modelled and Measured Structural Vibration Periods

Mode	Modelled period	Measured period	Measured damping ratio
1	0.63s	0.48 – 0.50s	1.8 – 3.5%
2	0.56s	0.45 – 0.48s	1.6 – 3.0%
3	0.48s	0.42 – 0.43s	N/A

3 Analysis

3.1 Seismic hazard and ground motion record selection

A Probabilistic Seismic Hazard Assessment (PSHA) was performed in OpenQuake (Pagani et al., 2014) utilising the Beauval et al., (2018) seismic hazard model and updating its catalogue with recent earthquakes in the region. The seismic hazard for the site location in Quito, Ecuador, shown in Figure 3 and uses average spectral acceleration, $AvgSA$, as the intensity measure for a period range interval from $0.2T^*$ to $3T^*$ as in Eads et al., (2015), where $T^* = 0.6s$ as is the mean of $T_1 = 0.63s$ and $T_2 = 0.56s$. A $V_{s,30} = 480\ km/s$ was used in the model to account for local soil effects. Four different intensities are shown in Figure 3 to understand the intensity values at code-required return periods for building assessments in Ecuador.

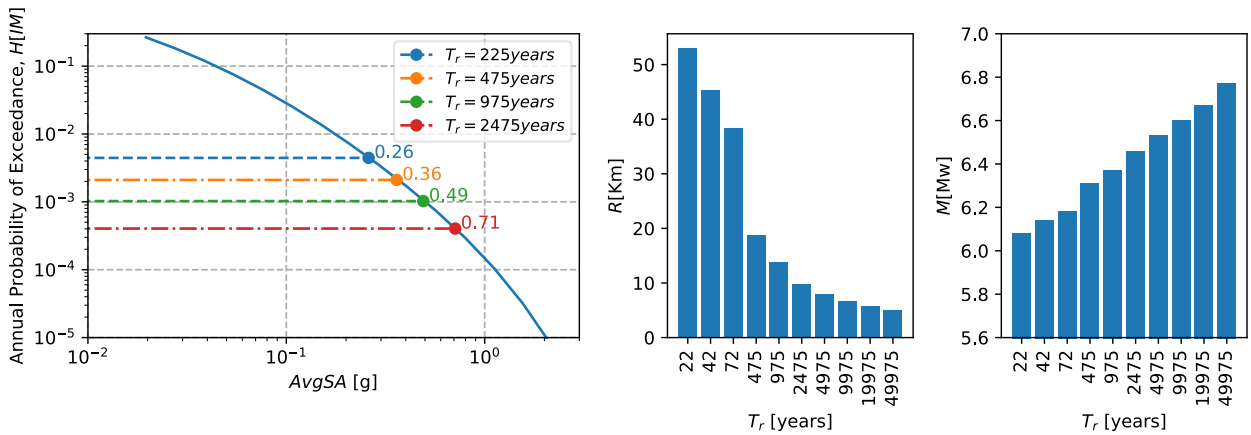

Figure 3. Seismic hazard curve (left) and disaggregation information (right) site location in Quito, Ecuador

Disaggregation for ten return periods spanning from 22 to 49975 years was performed to estimate *M* and *R* parameters for the construction of conditional spectra and record selection (Baker, 2011). Figure 3 also shows the mean values for each return period, in which *R* spanned from 53.0 Km to 5.0 Km and *M* spanned from 6.08 Mw to 6.77 Mw. Interestingly, the contribution for most of the analysed return periods is from sources less than 20 Km away which is the intra-slab failure system that crosses the city of Quito. Record selection was performed using open-source code (Ozsarac, 2022)using the NGA- West2 database (Ancheta et al., 2014). A total of 30 records per return period were selected with a maximum scale factor of 2.5.

3.2 Multiple stripe analysis

Using the records selected for each intensity level, Non-Linear Time History analysis (NLTH) was performed via Multiple Stripe Analysis (MSA) methodology (Jalayer, 2003). The benefits of MSA instead of other well-established techniques, such as Incremental Dynamic Analysis (IDA) proposed by Vamvatsikos (2002), are the compatibility of record selection with site hazard features via the conditional spectrum approach and the possibility of using limited scale factors for all intensity levels (Baker, 2015), helping avoid problems of response bias recently reported in the literature (Dávalos and Miranda, 2019). Results for displacements and accelerations were recorded at the structure's centre of mass, and Peak Storey Drift (PSD) and Peak Floor Acceleration (PFA) for each building level were computed. Residual Peak Storey Drift (RPSD) was also estimated, allowing the structure to free vibrate after the record ended. Structural collapse was defined as exceedance by 1.5 of the Collapse Prevention drift capacity, as defined by ASCE (2017), or when numerical non-convergence was reached.

The median EDPs are shown in Figure 4 for each considered intensity and structural direction conditioned on no collapse. Interesting to note is that the highest return period generates 100% collapses and is not shown. We can see from the PSD profiles that the X-direction is slightly more flexible and has higher drifts which is consistent with the period measurements and stiffness distribution on elements. Regarding PFA, it is possible to see some amplification on the top floors with reduced demands at mid-height. These acceleration peaks in the upper floors are due to higher mode effects, yielding at the base and vertical stiffness structural irregularity.

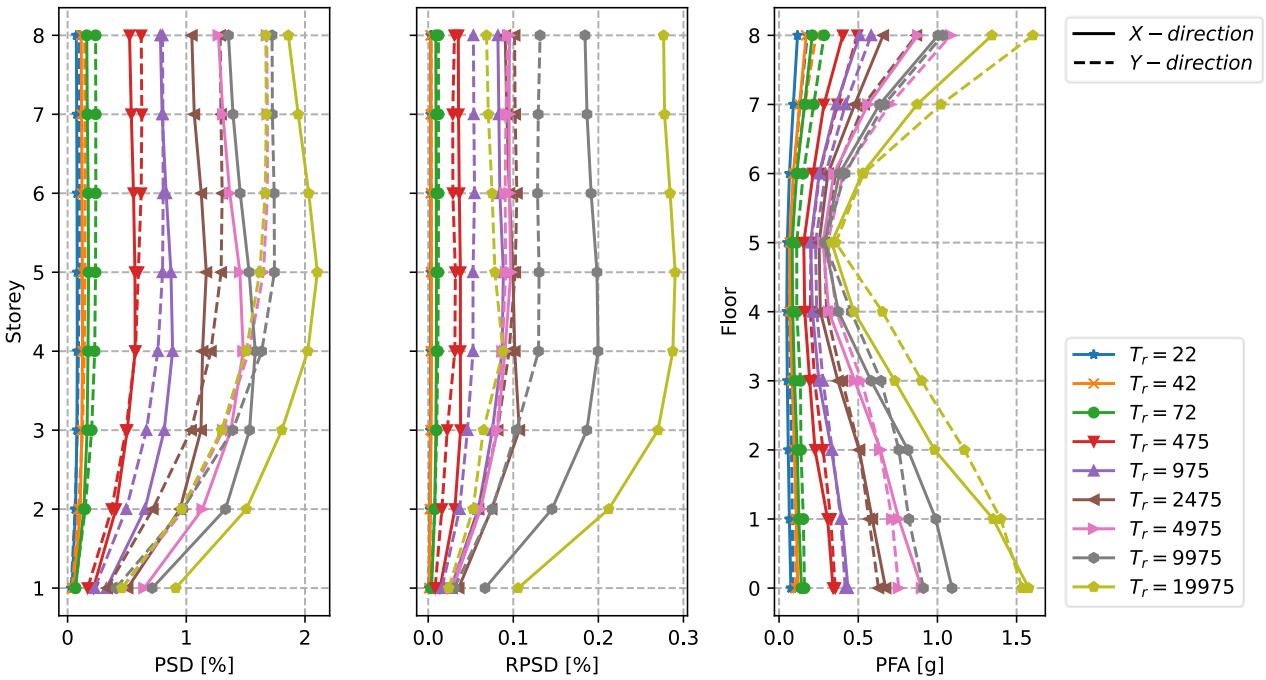

Figure 4. Median peak storey drift (PSD) [%], residual peak storey drift (RPSD) [%] and peak floor acceleration (PFA) [g] profiles at increasing return periods

3.3 Fragility functions

The fragility functions presented in Figure 5 were developed by fitting a cumulative distribution function for the exceedance of the different damage states that control the structural response, which was the shear wall

response. The first three damage states of the shear walls were defined as per ASCE 41 (2017) acceptance criteria tables for PSD-sensitive elements known as Immediate Occupancy (IO), Life Safety (LS) and Collapse Prevention (CP) in addition to the derived Collapse (C) damage state. At this point, it is possible to quickly note that the structure does not satisfy the code-based assessment since median values for LS and CP exceed 0.26g and 0.49g *AvgSA* intensities corresponding to 225 and 975 years return periods respectively as performance objectives for existing structures. Nevertheless, the collapse probability for the 975-year return period does not exceed the 10% threshold, as stated in the ASCE 7 (2017) provision. Moreover, a 10% collapse probability is exceeded for the 2475-year return period intensity if it were to be assessed as a new structure. Seismic collapse risk is computed as the annual rate of structural collapse by combining the hazard curve with the collapse fragility. Integrating the two, the mean annual frequency of collapse (MAFC) was found to be $\lambda_{col} = 0.375\text{e-}3$, corresponding to a return period of 2664 years. The MAFC is considerably larger than the limit suggested by ASCE 41-17 (2017), which is 1% in 50 years and corresponds to a 5000-year return period.

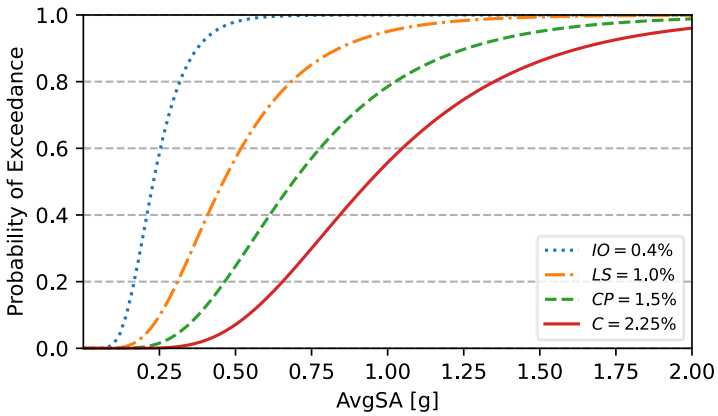

Figure 5. Fragility Functions, corresponding mean, and dispersion: $\theta_{IO} = 0.23, \beta_{IO} = 0.38$, $\theta_{LS} = 0.46, \beta_{LS} = 0.47$, $\theta_{CP} = 0.69, \beta_{CP} = 0.47$ *and* $\theta_C = 0.94, \beta_C = 0.43$

Figure 6. Distribution of the total repair costs among each storey in terms of PG and EDP

3.4 Derivation of storey loss functions

Storey Loss Functions (SLFs) were generated following the procedure described by Shahnazaryan et al., (2021), where Monte Carlo simulations are performed to generate a vulnerability function for each storey for each required EDP. In this case, PSD and PFA were the selected EDPs since they are the most common and have available fragilities in the literature for the NSEs. For the specific case of the underground floors catalogue, its contents were lumped into the ground floor. PSD-sensitive components were discarded since no underground significant drift is expected nor modelled. To clarify the repair costs distribution throughout the building height, Figure 6 shows the total value of the total repair costs for each storey and the percentage distribution per category or EDP sensitivity. From the repair cost distribution, it is possible to underline the relatively high value that NSE and contents have compared to the structural repair cost at the different storeys. A similar proportion between structural and non-structural components was shown by Taghavi and Miranda (2003) for the hotel typology. Moreover, since the ground floor and underground floors have a larger area and costly equipment required for the general operation of the entire hotel building complex, the lumped ground floor has the most significant repair cost value. It is seen that this is entirely due to the PFA-sensitive damage, further supporting the decision to either protect these valuable machinery dampers or isolation or through a more global bae isolation retrofit intervention strategy.

Figure 7 presents the SLFs for PSD-sensitive components for each structural orthogonal direction and separately shows the corresponding SLFs for PFA-sensitive components. In the case of PSD-sensitive SLFs, one direction has a higher repair cost value. This is explained by the fact that one-direction loading systems were standard for the typology and construction date under consideration. Moreover, strong infills coincide with the stiff direction of the columns, increasing the repair costs of the specific direction. Regarding the PFA-sensitive SLFs, it is evident that the ground floor represents a significant repair cost, given the location of many valuable pieces of equipment on the ground floor. Comparing losses of both types of EDPs, PFA losses are considerably higher than PSD losses. Another major contributor is that many building contents are assumed to be correlated to damage to the piping fragilities; hence, the damage and subsequent leakage of the piping is assumed to trigger extensive contents replacement across the building, which is a fair reflection of reality, considering this exact situation has been observed in past earthquakes such as the 1994 Northridge earthquake (Chavez and Binder, 1996)and the 2010 Chile earthquake (Miranda et al., 2012).

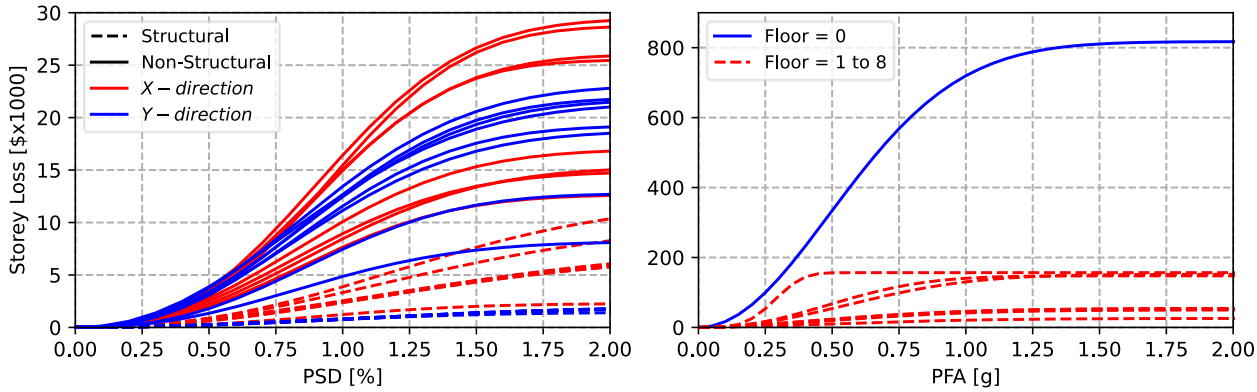

Figure 7. Drift-sensitive and acceleration-sensitive storey loss functions

3.5 Generalised storey loss functions

To facilitate the use of the SLFs for similar case studies, the obtained SLFs were normalised by the total repair cost for each storey as shown in Figure 6, which can be formalised in Equation 1.

$$E\left[\breve{\breve{L}}_T \mid NC \cap R\right]_{PG,i} = \frac{E[L_T \mid NC \cap R]_{PG,i}}{\sum_j E[L_T \mid NC \cap R]_{PG,j}} \quad (1)$$

where $E\left[\breve{\breve{L}}_T \mid NC \cap R\right]_{PG,\mathrm{i}}$ is the generalised expected repair cost of a particular Performance-Group (PSD or PFA-sensitive) and $NC \cap R$ simply refers to the assumption that the building has not collapsed and it is repairable. $E[L_T \mid NC \cap R]_{PG,\mathrm{i}}$ is the actual expected repair cost of the PG of interest (Figure 7) and $\sum_j E[L_T \mid NC \cap R]_{PG,\mathrm{j}}$ is the total repair cost considering all PGs in a single storey (Figure 6). Figure 8 presents

the generalised SLFs for the hotel building examined. This is a handy resource for practitioners since the generation of a detailed catalogue and SLFs can be avoided. One needs to evaluate the suitability of this normalised data to their specific context and scale the generalised SLFs via their specific total repair costs to have a representative set of SLFs. The critical thing to note is that the general trend of how economic losses are accumulated with increasing EDP is logical and representative; the relative value of these losses is then specified by the user when scaling them to their particular case study. Nevertheless, the limitations should be noted, such as the variability in the components, quantities, and repair costs which need to be evaluated from Table 1. Again, these generalised SLFs are available as an electronic supplement at: https://gerardjoreilly.github.io/publications/.

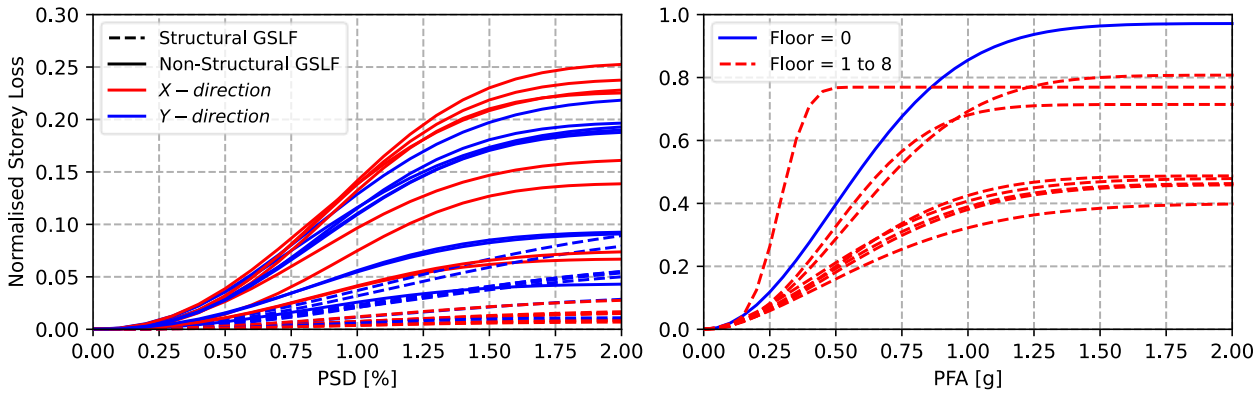

Figure 8. Generalised drift-sensitive and acceleration-sensitive storey loss functions

3.6 Loss estimation

The expected annual loss (EAL) for the building was calculated by combining vulnerability curves with the site hazard curve as given in Equation 2.

$$EAL = \int E[L_T \mid IM = im] \left| \frac{dH(IM > im)}{\mathrm{dim}} \right| \mathrm{dim} \tag{2}$$

where $E[L_T \mid IM = im]$ is the expected total economic loss or vulnerability defined in Equation 3.

$$\begin{aligned} E[L_T \mid IM = im] = {} & E[L_T \mid NC \cap R, IM = im](1 - P[D \mid NC, IM = im])(1 - P[C \mid IM = im]) \\ & + E[L_T \mid NC \cap D]P[D \mid NC, IM = im](1 - P[C \mid IM = im]) + E[L_T \mid C]P[C \mid IM = im] \end{aligned} \tag{3}$$

where the total economic loss is calculated by adding up the costs associated with three distinct, exhaustive events that are mutually exclusive. $E[L_T \mid NC \cap R, IM = im]$ is the expected repair cost at a given *im* conditioned on non-collapse and repairability of the building. $E[L_T \mid NC \cap D]$ is the expected replacement cost at a given *im* conditioned on non-collapse and the non-repairability of the building. $E[L_T \mid C]$ is the expected replacement cost due to collapse at a given *im*. $P[D \mid NC, IM = im]$ is the probability of requiring to demolition given non-collapse of the building at a given *im* due to excessive RPSD. $P[C \mid IM = im]$ Is the collapse probability at a given *im*.

Utilising the results of the dynamic analysis and SLFs described in previous sections, the expected losses for each return period and the EAL were estimated, as described by Shahnazaryan & O'Reilly (2021).

It is essential to mention that demolition was considered when 1.5% of residual peak storey drift (RSPD) was exceeded, as suggested by Ramirez & Miranda (2012). The total replacement cost is estimated by multiplying a surveyed replacement cost per square meter. This was estimated by local experts to be 995.77 \$/ m^2 and includes demolition costs. This unit value is then multiplied by the total area of the central block, including the underground floor area, which was computed as 6458.69 m^2. Figure 9 presents the vulnerability function of the hotel first in terms of the Expected Loss Ratio, which was normalised with total replacement cost to obtain the vulnerability function. Moreover, from the contribution of each case to the vulnerability, it is possible to note that non-structural losses have the highest contribution for low intensities and collapse for higher intensities. Demolition and structural repair costs are nearly negligible. Compared to Martins and Silva (2021), for

example, vulnerability data for a similar typology (CR_LWAL-DUM_H:7), slightly higher values for the expected losses of the present case study were found but were within the same overall range.

Figure 9 also presents the contributions to the EAL, which was computed to be 0.525% for this hotel building in Quito. The losses are dominated by the NSE contribution at lower intensities. It was reported that following previous low-intensity ground motions (i.e., 3<Mw<5) in the region, infill cracks were found during field inspections of the hotel building, and repairs were then carried out as general maintenance. This is essentially field evidence to support some of the observations presented here regarding the contributions of NSEs to losses in Figure 9. Compared to other values in the literature, the EAL for an 8-storey bare frame presented by Ramirez et al. (2012), showed a variation between 0.95% and 1.3%. Likewise, the EAL observed here aligns with values observed in Italian structures, as per O'Reilly and Sullivan (2018), for example.

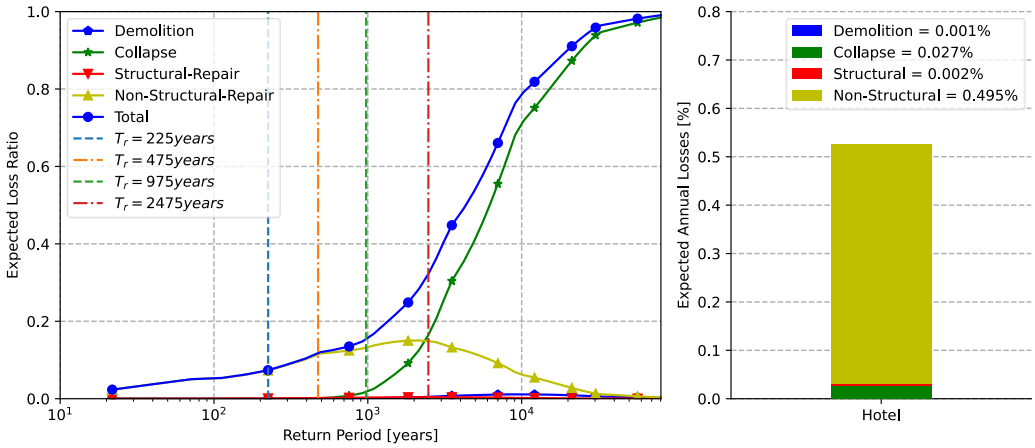

Figure 9. Vulnerability function and expected annual loss with the different contributions disaggregated

Figure 10 illustrates the disaggregation of repair losses for each of the eight storeys, categorized by EDP and for four return periods commonly referred to as the Design Earthquake and Maximum Considered Earthquake for new and existing structures. Notably, a significant impact of NSE on losses is observed, particularly on the ground floor (with lumped underground NSE) and the top floor. Repair losses add up to $478K, $765K, $873K and $975K, respectively, for each return period. These results highlight the location, importance and need of a NSE retrofitting.

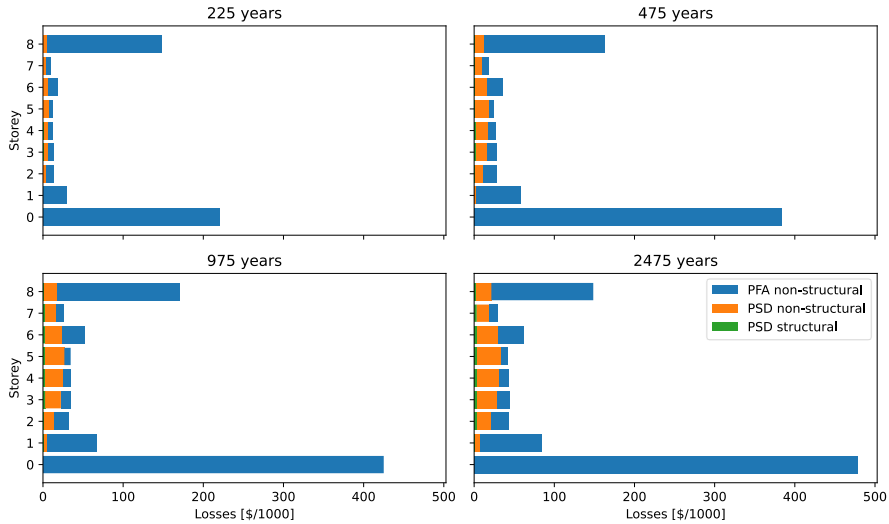

Figure 10. Storey repair losses at different return periods

4 Summary and conclusions

This paper presents a case study assessment of a hotel building in Quito, Ecuador, built in the late 1950s. The study underscores the importance of gathering diverse data sources, such as in-situ tests, ambient noise vibrations, and local expert insights, for a thorough seismic assessment. Ensuring the reliability of numerical modeling assumptions relies heavily on establishing correspondence with dynamic properties. This analysis captures the Engineering Demand Parameters (EDP) necessary for estimating repair costs. Additionally, the study compiles a list of damageable components based on input from building owners and local experts, complete with corresponding fragilities and repair cost data to build storey loss functions (SLFs), which were then normalised for general use. The research also establishes structural fragilities according to ASCE 41 (2017) criteria and calculates vulnerability and Expected Annual Losses (EAL), providing valuable insights for decision-makers. The main conclusions of this study are as follows:

- Observations reveal that the hotel's performance falls below contemporary standards, a common challenge in the local and regional context. Decision-makers are urged to evaluate collapse probabilities based on both national standards and their own risk objectives.
- The vulnerability and loss assessment not only estimate decision values but also identify key contributors, facilitating the development of strategic retrofit solutions.
- The study highlights the effectiveness of Storey Loss Functions (SLFs) in providing reliable quantifications for detailed loss assessments. Additionally, the potential applicability of Generalized Storey Loss Functions (GSLFs) is recognized as a significant contribution.

In essence, this case study serves as a valuable reference for seismic loss assessments, particularly for structures not meeting code compliance standards. The research aims to inform decision-making regarding seismic retrofitting in Ecuador and the broader South American context, contributing to enhanced resilience against seismic risks.

Acknowledgements

The authors would like to sincerely thank the property owners and the local experts for their cooperation and support during this work. Their contributions and insights were essential to the success of this research. The work presented in this paper has been developed within the framework of the project "Dipartimenti di Eccellenza 2023-2027", funded by the Italian Ministry of Education, University and Research at IUSS Pavia.

References

ACI Committee 318 (2019). *Building Code Requirements for Structural Concrete (ACI 318-19) and Commentary (ACI 318R-19* Farmington Hills, MI: American Concrete Institute.

Ancheta T.D., Darragh R.B., Stewart J.P., Seyhan E., Silva W.J., Chiou B.S.-J., Wooddell K.E., Graves R.W., Kottke A.R., Boore D.M. (2014). NGA-West2 database, *Earthquake Spectra*, 30(3): 989–1005.

ASCE/SEI 7-16 (2017). *Minimum Design Loads and Associated Criteria for Buildings and Other Structures*[Online] American Society of Civil Engineers. Available from: https://ascelibrary.org/doi/abs/10.1061/9780784414248.

ASCE/SEI 41-17 (2017). *Seismic Evaluation and Retrofit of Existing Buildings*[Online] Reston, VA: American Society of Civil Engineers. Available from: https://ascelibrary.org/doi/abs/10.1061/9780784414859.

Baker J.W. (2011). Conditional Mean Spectrum: Tool for Ground-Motion Selection, *Journal of Structural Engineering*, 137(3): 322–331.

Baker J.W. (2015). Efficient analytical fragility function fitting using dynamic structural analysis, *Earthquake Spectra*, 31(1): 579–599.

Beauval C., Marinière J., Yepes H., Audin L., Nocquet J. -M., Alvarado A., Baize S., Aguilar J., Singaucho J. -C., Jomard H. (2018). A New Seismic Hazard Model for Ecuador, *Bulletin of the Seismological Society of America*,.

Calabrese A., Almeida J.P., Pinho R. (2010). Numerical issues in distributed inelasticity modeling of RC frame elements for seismic analysis, *Journal of Earthquake Engineering*, 14(S1): 38–68.

Chavez C.W., Binder B. (1996). A hospital as victim and responder: The Sepulveda VA Medical Center and the Northridge earthquake, *Journal of Emergency Medicine*, 14(4): 445–454.
Dávalos H., Miranda E. (2019). Evaluation of the scaling factor bias influence on the probability of collapse using SA(T1) as the intensity measure, *Earthquake Spectra*, 35(2): 679–702.
Eads L., Miranda E., Lignos D.G. (2015). Average spectral acceleration as an intensity measure for collapse risk assessment, *Earthquake Engineering & Structural Dynamics*, 44(12): 2057–2073.
FEMA P-58 (2018). *Seismic performance assessment of buildings*
Jalayer F. (2003). *Direct Probabilistic Seismic Analysis: Implementing Non-Linear Dynamic Assessments*.
Mander J.B., Priestley M.J.N., Park R. (1988). Theoretical Stress-Strain Model for Confined Concrete, *Journal of Structural Engineering*, 114(8): 1804–1826.
Martins L., Silva V. (2021). Development of a fragility and vulnerability model for global seismic risk analyses, *Bulletin of Earthquake Engineering*, 19(15): 6719–6745.
Miranda E., Mosqueda G., Retamales R., Pekcan G. (2012). Performance of Nonstructural Components during the 27 February 2010 Chile Earthquake, *Earthquake Spectra*, 28(S1): S453–S471.
Nafeh A.M.B., O'Reilly G.J. (2023). Simplified pushover-based seismic loss assessment for existing infilled frame structures, *Bulletin of Earthquake Engineering*,.
NEC-15 (2014). *Norma Ecuatoriana de la Construcción - NEC: NEC-SE-DS - Peligro Sísmico/Diseño Sismo Resistente*[Online] Ministerio de Desarrollo Urbano y Vivienda. Available from: https://www.habitatyvivienda.gob.ec/documentos-normativos-nec-norma-ecuatoriana-de-la-construccion/.
Odabaşı Ö. (2020). *Probabilistic Seismic Risk Analysis of High-Rise Buildings: Critical Considerations in Site-Specific and Regional Applications*.
O'Reilly G.J., Sullivan T.J. (2018). Probabilistic seismic assessment and retrofit considerations for Italian RC frame buildings, *Bulletin of Earthquake Engineering*, 16(3): 1447–1485.
Ozsarac V. (2022). EzGM: Toolbox for ground motion selection and processing, *Zenodo*,.
Pagani M., Monelli D., Weatherill G., Danciu L., Crowley H., Silva V., Henshaw P., Butler L., Nastasi M., Panzeri L. (2014). OpenQuake engine: An open hazard (and risk) software for the global earthquake model, *Seismological Research Letters*, 85(3): 692–702.
Ramirez C.M., Liel A.B., Mitrani-Reiser J., Haselton C.B., Spear A.D., Steiner J., Deierlein G.G., Miranda E. (2012). Expected earthquake damage and repair costs in reinforced concrete frame buildings, *Earthquake Engineering and Structural Dynamics*, 41(11): 1455–1475.
Ramirez C.M., Miranda E. (2012). Significance of residual drifts in building earthquake loss estimation, *Earthquake Engineering and Structural Dynamics*, 41(11): 1477–1493.
Scott M.H., Fenves G.L. (2006). Plastic hinge integration methods for force-based beam–column elements, *Journal of Structural Engineering*, 132(2): 244–252.
SeismoSoft (2023). SeismoStruct—a computer program for static and dynamic nonlinear analysis of framed structures,
Shahnazaryan D., O'Reilly G.J. (2021). Integrating expected loss and collapse risk in performance-based seismic design of structures, *Bulletin of Earthquake Engineering*, 19(2): 987–1025.
Shahnazaryan D., O'Reilly G.J., Monteiro R. (2021). Story loss functions for seismic design and assessment: Development of tools and application, *Earthquake Spectra*, 37(4): 2813–2839.
Taghavi S., Miranda E. (2003). *Response Assessment of Nonstructural Building Elements*
Vamvatsikos D., Allin Cornell C. (2002). Incremental dynamic analysis, *Earthquake Engineering and Structural Dynamics*, 31(3): 491–514.